



# Error propagation in nuclear models

Author: Artis Muceniaks

---

Thesis submitted for the degree of  
Bachelor of Science, 15 Ects

Supervisor: Andrea Idini, Gillis Carlsson

Examiner: Claudio Verdozzi

Department of Physics  
Division of Mathematical Physics  
December 2022

### **Acknowledgments**

I would like to thank my advisors Andrea Idini and Gillis Carlsson for being very patient and sacrificing a lot of time to help me. They have been encouraging through and through, showing me how to develop a greater understanding of physics and applying the acquired physical understanding also to problems beyond physics.

## Abstract

In this thesis we perform error analysis of a nuclear model based on density-functional theory developed in Lund. The Lund model allows us to perform calculations of nuclear spectra more efficiently by constructing a simple effective Hamiltonian reproducing the quadrupole deformation and pairing interaction strength parameters of a spherical Hartree-Fock reference functional. This constraining of the Hamiltonian allows for more efficient computation. The spectra calculated using Beyond mean-field methods to solve the effective Hamiltonian involve approximations. This work allows us to quantify the uncertainties in the model using statistical methods. In particular, we perform a propagation of errors and covariance analysis to determine the parameters which contribute most to the uncertainties of the calculations of energy spectra  $E$  and separation energies  $T$ .

The covariances calculated indicate that  $E$  and  $T$  are largely uncorrelated for low spin states, where as spin  $I = 4$  shows a larger degree of covariance. Through statistical analysis, we identify that the major contribution to the errors comes from the choice of the pairing parameter, but the magnitude of this contribution decreases for states with larger spin. We speculate that the different parameter sensitivities of states with spin  $I = 2, 4$ , can be explained by different deformations in spinning states which lead to a breaking of time-reversal symmetry, which leads to a decreased dependence on the pairing parameter  $g$ .

# Contents

<b>1</b>	<b>Introduction</b>	<b>2</b>
<b>2</b>	<b>Method</b>	<b>4</b>
2.1	Effective Hamiltonian . . . . .	4
2.2	Calculation of spectra . . . . .	5
2.3	Statistical methods . . . . .	7
2.3.1	Covariance . . . . .	8
<b>3</b>	<b>Results</b>	<b>10</b>
3.1	Variance of individual parameters . . . . .	11
3.1.1	Variation in $\chi$ . . . . .	11
3.1.2	Variation in $g$ . . . . .	13
3.2	Covariance of $\chi$ and $g$ . . . . .	14
<b>4</b>	<b>Conclusion and Outlook</b>	<b>18</b>

## Abbreviations

**HF:** Hartree-Fock

**HFB:** Hartree-Fock-Bogoliubov

**DFT:** Density-functional theory

**EFT:** Energy-functional theory

# 1 Introduction

The theoretical modeling of atomic nuclei has proven to be a challenging area of research in quantum many-body physics. The nucleus is a complex system of protons and neutrons interacting predominantly through the very short range strong interaction and the long range Coulomb interaction [1]. The large number of particles and the self-bound nature of the nucleus has as a consequence that calculations from quantum first principles, considering every possible interaction between nucleons, are exceptionally computationally intensive, requiring millions of CPU-hours for moderately sized nuclei [2]. The computational requirements combined with our limited understanding of nucleon-nucleon forces has made *ab initio* approaches unfeasible for heavy deformed nuclei [3]. This has forced nuclear models to use phenomenological considerations to simplify the calculations.

Phenomenological models reduce the complexity of the calculations. Basing the model on quantum theory, parameters are fit to reproduce experimental data directly in nuclei. This has been used starting with early nuclear models like the liquid drop model, conceiving the nucleus as a liquid with surface and volume contributions to the energy [1], up to modern approaches like mean-field and beyond mean-field methods.

Mean-field methods, such as the Hartree-Fock method, mentioned in this thesis, reduce the complexity of calculations by reducing individual many-body interactions to an interaction of a particle with a average potential arising from all other particles in the system. Take as an example the Skyrme interaction, which approximates the nucleon-nucleon interaction as a density dependent functional, that is a function of nucleon, kinetic energy and spin-orbit densities. The mathematical form of the Skyrme interaction, is expressed in terms of  $\delta$ -function contact interactions, with a two-body density dependent term, which simplifies the calculations enormously [4, 5].

As there are between 6-12 free parameters in the Skyrme interaction it is not possible to determine the overall best parameters [3]. In fact there are a number of parameterizations optimized for reproduction of specific observables—nuclear binding energies, shapes and energy level differences—across the nuclear landscape [3, 6, 7].

Despite the sophistication of these models, and unlike in some other areas of research, there are still large disagreements between theory and experiment [8]. For example energies calculated using mean-field approaches can have a discrepancy with experiment on the order of 1 MeV, compared to experiments where the precision reaches the keV or even the eV scale [9]. This is where the need for error estimates for these models arises [8, 10].

By performing statistical and correlation analysis as well as considering the underlying assumptions of the phenomenological models, one can arrive at error estimates for the computed values. By calculating these error estimates alongside the observables, we can acquire a deeper insight into the performance, limitations and possible missing physics in the methods used [8].

Through a statistical analysis of a model, varying the parameters and performing calculations, one can estimate among other things the degree to which parameters are constrained and their errors, assess the performance of the model's extrapolation capability and how the observables depend on each other, which is a useful guide to understanding the underlying physics [8]. Despite current nuclear theoretical calculations showing large discrepancies from experimental observations, they still play a key role in many research areas. Therefore theoretical model error analysis can play a role in furthering experimental nuclear physics.

The experimental search for super-heavy nuclei involves spectroscopy of products of fusion reactions. These can be guided by theoretical estimates of transition energies which are then matched to experimental data. By comparing the spectroscopy data to theoretical predictions one can try to identify the nuclei involved [11]. The production of super-heavy nuclei involves processes with very small interaction cross sections, therefore it is in the interest of experimental nuclear physicists to have accurate estimates for particularly stable nuclei. The so called magic nuclei are more tightly bound and could be targets for experiments trying to produce nuclei at the extremes of the nuclear landscape [11].

Nuclear Theory error estimates could also be useful for astrophysics research, as stellar models rely on information about neutron-rich nuclei far from those possible to observe in a laboratory setting. Better understanding of these nuclei could inform research on the  $r$ -process and give insight into the nature of nucleosynthesis in the Galaxy [12]. There is already research applying the statistical methods outlined above to optimize mean-field models by including neutron star data [13].

Error analysis is crucial to interpreting scientific findings. Error propagation has been fruitful across research areas from atomic physics to global climate models. The error analysis of nuclear models has grown in popularity in the past decade. The quantification of errors stemming from calculation errors, parameter estimation and model discrepancies, such as truncation errors, are seen as essential for progress in precision calculation in energy-functional theory (EFT) nuclear physics [14].

The main tools in the error analysis are those of standard statistics. Using covariance and sensitivity analysis we can quantify the statistical significance of changes of our observables as the parameters change [15]. In particular, diagonalizing the covariance matrix gives a wealth of information of the correlated parameters, as seen for example in analysis performed to give an error estimate of the neutron skin thickness of lead [16].

In this thesis we want to apply statistical methods to analyze the results by the recent framework to model nuclear spectroscopic properties of Ljungberg et al. [9] which uses mean-field and beyond mean-field methods to determine an effective nuclear Hamiltonian, which is then used to calculate observables of interest.

The following section will cover the definition of the effective Hamiltonian used in the model, an introduction to the framework and notes on statistical methods useful for our analysis.

## 2 Method

### 2.1 Effective Hamiltonian

The system is described by an effective Hamiltonian  $\hat{H}$  that is chosen to consist of three components [9],

$$\hat{H} = \hat{H}_0 + \hat{H}_Q + \hat{H}_P, \quad (1)$$

where  $\hat{H}_0$  is the spherical single particle potential,  $\hat{H}_Q$  is the quadrupole-quadrupole interaction and  $\hat{H}_P$  is the neutron-neutron and proton-proton pairing interaction.

The spherical single particle potential expressed in the creation ( $a_i^\dagger$ ) annihilation  $a_i$  operator form is written as

$$\hat{H}_0 = \sum_i e_i a_i^\dagger a_i + E_0, \quad (2)$$

which expresses the average interaction between the nuclei, described by the set of quantum numbers  $i \equiv (q_i n_i l_i j_i m_i)$ . Here  $q_i$  is the particle species (neutron/proton),  $n_i$  the principal quantum number,  $l_i$  angular momentum and  $j_i, m_i$  the total angular momentum and its projection respectively.  $E_0$  and  $e_i$  are a constant energy and single particle energy values respectively [9]. The  $\hat{H}_0$  is determined by a spherical Hartree-Fock (HF) calculation with a reference Skyrme functional in part 2 of the computation.  $E_0$  is an energy constant selected such that it reproduces the binding energy (lowest point in Fig. 1) of the HF calculation.  $e_i$  are the single particle energies associated with the  $i$  HF orbitals [9].

The quadrupole interaction encodes the quadrupole operator  $\hat{Q}$  deformation energy.

$$\hat{H}_Q = \chi \sum_\mu \hat{Q}_\mu^\dagger \hat{Q}_\mu \quad (3)$$

With the coupling strength parameter  $\chi$  that is fitted to reproduce the deformed HF solution from part 1 of the calculation (Fig. 1). The quadrupole operators used here are adjusted by a Woods-Saxon form factor,  $\hat{Q}_\mu = f(r) Y_\mu^2(\hat{r})$  [17], where  $r$  is the radial distance of the nucleon from the center of the potential and  $\hat{r}$  is the vector pointing to the nucleon from the center of the potential.

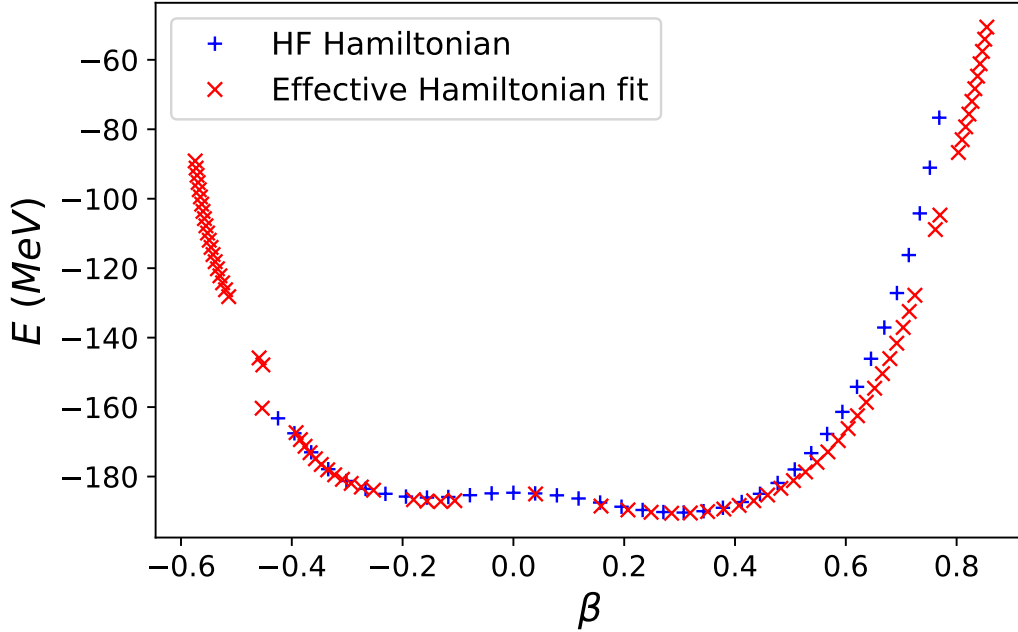


Figure 1: Comparison of Hartree-Fock ground state energies for the nucleus  $^{24}\text{Mg}$  at different quadrupole deformations  $\beta$ , obtained with the Skyrme energy density functional SLy4 (blue pluses) and the effective Hamiltonian SLy4-H (red crosses) described in Eq. (1).

The last part of the Hamiltonian is the pairing term,

$$\hat{H}_P = g\hat{P}^\dagger\hat{P}. \quad (4)$$

Here  $g$  expresses the pairing coupling strength and  $\hat{P} = a_i^\dagger a_{\bar{i}}^\dagger a_j a_{\bar{j}}$  is the pairing operator which expresses the energy of two paired particles in time reversal state  $\hat{i}$  being moved between energy levels  $i, j$ .

## 2.2 Calculation of spectra

The method of calculation is divided into 6 parts.

- part 1: A constrained Hartree-Fock (HF) calculation of the deformation energy using the Skyrme interaction.
- part 2: Generation of operators and Hartree-Fock basis states for the effective Hamiltonian.
- part 3: Fitting of the quadrupole deformation strength in the effective Hamiltonian.
- part 4: A calculation of the Hartree-Fock-Bogoliubov (HFB) basis states calculated using the generator coordinate method (Fig. 2).
- part 5: Combining of the HFB basis states restoring the broken symmetries.

- part 6: Calculation of spectra by solving the Hill-Wheeler equations.

HF and HFB are variational methods for calculating many-body wave functions through reducing the many-body interactions to average potentials. The HFB method additionally includes an average potential expressing the pairing interaction, which is a force that can be understood by considering spatial overlap of densities between two nuclei. The Skyrme force we use as the single particle potential is a phenomenological interaction fitted to experimental data [4].

Crucially, both the variational methods and the effective Skyrme force are approximations. The variational methods take as their starting point a set of single particle trial functions (i.e. the spherical harmonics), and by minimizing an energy value through varying the single particle state densities converge to an approximation of the many-body wave function. This leaves room for errors to accumulate throughout the calculations.

We then use the effective Hamiltonian with the HFB method to find basis states by minimizing the HFB equations for a selection of radial deformation values  $\gamma$ ,  $\beta$ , neutron and proton pairing strengths  $g_p, g_n$  and rotational frequency of the nucleus (cranking frequency)  $j_x$ . The sample space for the deformations and their respective lowest energies can be seen in Fig. 2. This gives us a set of symmetry broken HFB states  $|\text{HFB}_i\rangle$ . These states being symmetry broken means that neither the number of nucleons or angular momentum are good quantum numbers [9]. To fix this the states need to be mixed and projected to restore symmetries. By projecting the states using the neutron/proton number and angular momentum projection operators giving our final wave functions  $|\Psi_i\rangle$  in part 5 of the modeling.

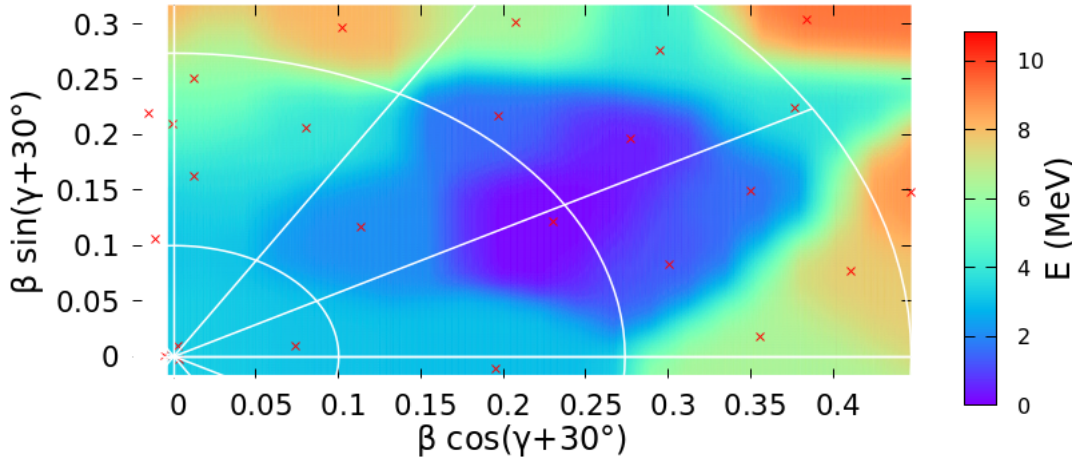


Figure 2: The deformation sampling points for  $^{24}\text{Mg}$ . The color representing the HFB energy in MeV for a computation with 4 oscillator basis from SLy4 effective interaction.

The spectra are then calculated in part 6 of the model by solving the Hill-Wheeler equation

$$\hat{H}h = E\hat{O}h, \quad (5)$$

Where the operator  $\hat{O}_{ij} = \langle \Psi_i | \Psi_j \rangle$  is used to take care of the non-orthogonality of the HFB states. and the matrix elements of  $\hat{H}$  and the energies  $E$  are calculated by the symmetry restoration procedure.

### 2.3 Statistical methods

Given the fact that density functional approaches used in the first two parts of the model use assumptions, approximations and fitting to experimental data, there are limitations to the accuracy of the calculated spectra. The model we use can have statistical model errors due to the fitting procedures which affect the coupling constants. For these reasons one might want to find confidence intervals for the parameters determined by fitting and observe how the results vary throughout the range of reasonable parameter values [8]. As the effective Hamiltonian parameters  $\chi$  and  $g$  we investigate are calculated by fitting to reference functionals, we can propagate the errors to the final observables.

There is a large variety of methods for analysis of that can be used to calculate, among other things, the maximum accuracy, the parameters whose variation effects the end results the most, the confidence intervals as the model is extrapolated to experimentally unknown values. Calculation of covariance matrices between the parameters defining the model could tell us whether the model is over or under-constrained and whether adding more data when deciding parameter could improve the model [8].

The initial fit of the parameters is done by minimizing the objective function by varying the parameters  $\mathbf{x}$  [8]. This is a function of a number  $N$  of observables  $\mathcal{O}_i$  being fit against.

$$\chi^2(\mathbf{x}) = \sum_{i=1}^N \frac{(\mathcal{O}_i(\mathbf{x}) - \mathcal{O}_i^{ref})^2}{\Delta \mathcal{O}_i^2}. \quad (6)$$

Within the analysis performed in this thesis the function  $\mathcal{O}(\mathbf{x})$  is a calculation using the effective Hamiltonian, while  $\mathcal{O}^{ref}$  come from calculations done using the reference functional [9]. The value  $\Delta \mathcal{O}$  is a value that quantifies the errors in our model arising from the above mentioned assumptions, approximations and eventually experimental errors. The fit determining  $\chi$  can be seen in Fig. 1.

The following analysis is performed by computing an observable  $\mathcal{O}$  for a set of numerical values of a variable  $x$  around the value  $x_0$  determined through the fitting procedure. To make meaningful comparisons between variables, whose typical values can vary by orders of magnitude, we scale the values of the variable to a percentage variation  $\tilde{x}$  by dividing with the value  $x_0$ :  $\tilde{x} = x/x_0$ . We also define the standard deviation as,

$$\sigma_{\tilde{x}} = \Delta \tilde{x} \left. \frac{\partial \mathcal{O}}{\partial \tilde{x}} \right|_{\tilde{x}_0}. \quad (7)$$

Here the value  $\Delta \tilde{x}$  is a scaling factor which describes a reasonable range of values for the variable. We chose the scaling  $\Delta \tilde{x} = 0.1$  for both  $\chi$  and  $g$  as 10% is a reasonable range for both  $\chi$  and  $g$

to vary within the fitting procedures, depending on the parameters chosen in part 1 and 2 of the model.

### 2.3.1 Covariance

Covariance is used to quantify the relationship between a set of variables  $\mathbf{x}$  and observables  $\mathbf{A}$ . The covariance between  $\mathbf{x}$  can be expressed in terms of the expectation values of the computed set of observables [18]. For example by varying the parameter  $\chi$  and  $g$  and then calculating the energy levels  $E = E(\chi, g)$  we can calculate the covariance of  $\chi$  and  $g$  which would express the degree of change of  $E$  as  $\chi$  and  $g$  are varied simultaneously.

The covariance can be calculated from the statistical properties of two sets  $A$  and  $B$ . These could be sets of experimental data points or calculations from a theoretical model. This value quantifies how the distances between points vary over the set of a number of points.

$$\text{cov}(A, B) = \frac{1}{M} \sum_{m=1}^M \left[ (A^{(m)} - \langle A \rangle)(B^{(m)} - \langle B \rangle) \right] = \langle AB \rangle - \langle A \rangle \langle B \rangle. \quad (8)$$

Here  $M$  is the dimension of both sets,  $\langle A \rangle$  and  $\langle B \rangle$  are the means of the sets and,  $A^{(m)}$ ,  $B^{(m)}$  elements of the sets. A positive covariance means that the quantities increase together, while a negative covariance means the values of one of the quantities decreases with an increase in the other. A smaller value of covariance implies weakly correlated dependence of the quantities between each other. We will consider the quantities to be the observables with respect to a variation in the parameters of the model  $\chi$  and  $g$ .

The covariance of an observable to changes in parameters can also be expressed in terms of derivatives of the observable by considering the quadratic expansion of its function around the mean  $\mathbf{x}_0$  of the set of parameters. Calculating the Jacobian  $\mathbf{J}$  for a set of observables  $\mathcal{O}_i$  and parameters  $x_\alpha$ ,

$$J_{i\alpha} = \left. \frac{\partial \mathcal{O}_i}{\partial x_\alpha} \right|_{\mathbf{x}_0}, \quad (9)$$

and assuming linearity allows us to approximate the Hessian [8],

$$\mathcal{C} = \mathcal{M}^{-1} \approx (\mathbf{J}^T \mathbf{J})^{-1}. \quad (10)$$

This expansion under the assumption of linearity lets us approximate the covariance as  $\mathcal{C} = \mathcal{M}^{-1}$  [8, 19]. In the case with two parameters and one observable to avoid having a singular matrix we need to approximate the second derivative by a finite difference, as done in section 3.2. After having calculated the Hessian we can then calculate the total error due to changes in many variables by a weighted sum over the terms in the Hessian  $\mathcal{M}$  similar to Eq. (7). In our model with two parameters this gives the total variance,

$$\sigma^2 = \left( \Delta \tilde{\chi} \frac{\partial \mathcal{O}}{\partial \tilde{\chi}} \right)^2 + \left( \Delta \tilde{g} \frac{\partial \mathcal{O}}{\partial \tilde{g}} \right)^2 + 2 \Delta \tilde{\chi} \Delta \tilde{g} \frac{\partial^2 \mathcal{O}}{\partial \tilde{\chi} \partial \tilde{g}}, \quad (11)$$

which corresponds to the linear extrapolation of the error propagation in change of the observable with a variation of  $\Delta\chi$  and  $\Delta g$  around the mean.

The covariance matrix gives a range of information about the distribution of our parameters. The diagonal entries are the variances of individual model parameters and the statistical error related to the determination of the parameter [8]. Fig. 3 shows a covariance ellipsoid, which is a way to visualize the variation of two parameters. The Quadratic expansion can be expressed for the case we are considering with two parameters  $\chi$  and  $g$  and observable  $E$  to be

$$Q = \begin{pmatrix} g - g_0 & \chi - \chi_0 \end{pmatrix} \mathcal{M} \begin{pmatrix} g - g_0 \\ \chi - \chi_0 \end{pmatrix}. \quad (12)$$

The ellipsoid, centered around  $\mathbf{x}_0$ , then bounds a region of parameters  $Q = k$  from the mean [19]. The direction of the ellipses semi-axis are defined by the eigenvectors  $\mathbf{e}_\alpha$  of the covariance matrix and the square root of the eigenvalues  $\lambda_\alpha$  define the semi-radii of of the ellipse [19]. The quantity  $Q = 1$ , defining the ellipse contour bounds an area of  $\sigma$ , where  $\sigma$  is the change in an observable we define in Eq. (11) [15, 19].

We can see the difference between the error estimate along the line at  $X_{02}$  on the plot which is an error estimate taking into account only the variation in one parameter (Eq. (7)) and the error estimate  $\Delta X_2$  calculated taking into account the covariance of two parameters (Eq. (11)), therefore being larger.

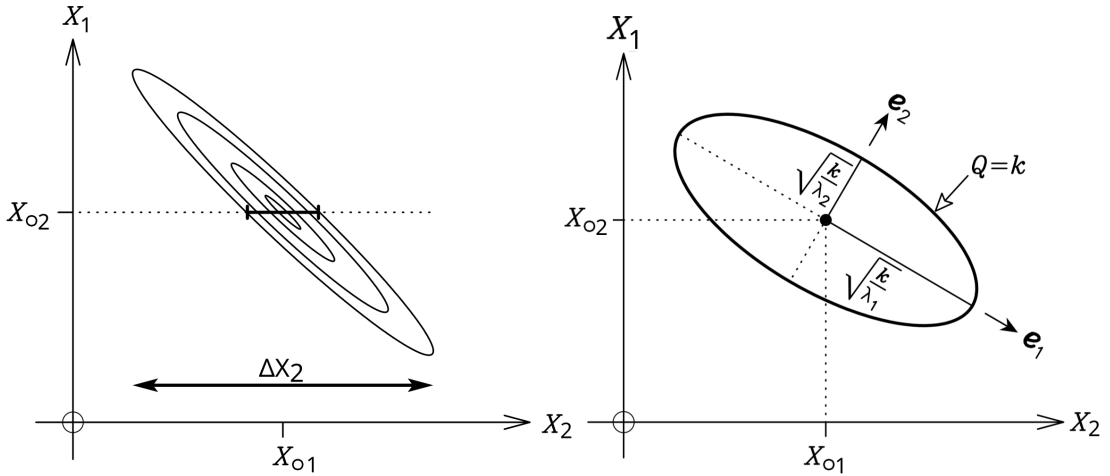


Figure 3: Example of a covariance ellipsoid for a model of two parameters. Adapted from Sivia and Skilling [19].

A useful measure of the correlation between two parameters is the Pearson correlation coefficient,

$$\rho_{\alpha\beta} = \frac{|\text{cov}(x_\alpha, x_\beta)|}{\sigma_{x_\alpha} \sigma_{x_\beta}}, \quad (13)$$

which ranges from  $-1$  to  $1$ ,  $1$  or  $-1$  meaning that the parameters  $x_\alpha$  and  $x_\beta$  are fully correlated or anti-correlated respectively and  $0$  meaning fully uncorrelated [8].

### 3 Results

The thesis consists of performing calculations using the model defined in sections 2.1 and 2.2. Apart from the parameters we consider in our statistical analysis the model has a number of additional computational parameters. Parameters such as the number of harmonic oscillators used as basis, number of HFB basis states  $N_{points}$  which are combined in the generator coordinate method to produce the final wave function as described in section 2.2, and various parameters having to do with the numerical integration performed across the calculations. All of these parameters affect the precision of the calculations. The number of Harmonic oscillator basis  $N_{max}$  for example impacts the ability of the model to reproduce physical phenomena. The parameters used in the following calculations are summarized in Table 1. The parameters  $n\theta$  and  $n\phi$  have to do with the number of integration points in part 5 of the calculation.  $\epsilon$  is a truncation parameter also in part 5 of the model.

$N_{max}$	4, 6
$N_{points}$	10, 50
$n\theta$	10
$n\phi$	24
$\epsilon$	$10^{-6}$

Table 1: Computational parameters for the performed calculations.

As one of the ways that varying the pairing strength  $g$  manifests in the spectrum is the energy difference between the first  $0^+$  states, we need to select a large enough model to have physical results, while keeping it small enough to perform the calculations in reasonable time. Calculating the spectra using 8 oscillator basis and 50 HFB basis points, a single calculation takes 3 hours running in the cluster<sup>1</sup> on 10 nodes of 40 processors. Reducing the number of oscillator basis to 6 a calculation takes 90 minutes, while still reproducing all the physical phenomena relevant for this analysis.

The nucleus modeled in all of the following calculations is  $^{24}\text{Mg}$  as it consists of a few nucleons, making the computation faster, while being notably deformed, which is of interest as the parameter  $\chi$  is fit to the quadrupole deformation.

---

<sup>1</sup>The computations were initially performed on a Linux machine locally. The code written in Fortran, appeared to have many numerical instability issues when compiled using the Gfortran compiler. The model was stable for a small number of  $N_{max}$ , but at  $N_{max}$  larger than 4 it failed to converge on any results. This was temporarily fixed by increasing truncation limits  $\epsilon$  in part 5 of the calculations which combine the HFB states. This allowed us to perform calculations with 6 oscillator basis, but was still unstable for larger grids of HFB states. The issue was solved by performing all the computation on the cluster, which was much more stable.

### 3.1 Variance of individual parameters

The first part of the analysis consists of variance calculations for the individual model parameters  $\chi$  and  $g$ , manipulating the quadrupole-quadrupole and pairing respectively. The parameters are varied over a range of values selected such that there are enough points to allow for fitting, while keeping them as low as possible due to the long calculation time. The spread of values is chosen so as to include the of the range of values that might result from the fitting procedures in part 1, 2 and 3 of the model.

#### 3.1.1 Variation in $\chi$

The first parameter varied is  $\chi$ . Fig. 4 shows 50 calculations for a range of  $\chi$  varied over 8% around the mean value of  $\chi$ . We see that the energy levels are linear and negatively correlated with  $\chi$  for most energy levels. The effect of numerical errors arising from the number of selected spherical-harmonic basis functions  $N_{max}$  can be seen for the nuclear angular momenta of  $I = 3, 4$  where there are small discontinuities in the way energy varies. The left panel of Fig. 5 shows how non-linear the energies are for  $I = 3$  for  $N_{max} = 4$ , compared to the level for  $I = 0$  in Fig. 4. The strong non-linearities come from a small variation of  $E$ . However, odd spin shows more numerical errors in calculations, so we chose to not consider the odd spins in all the rest of the calculations.

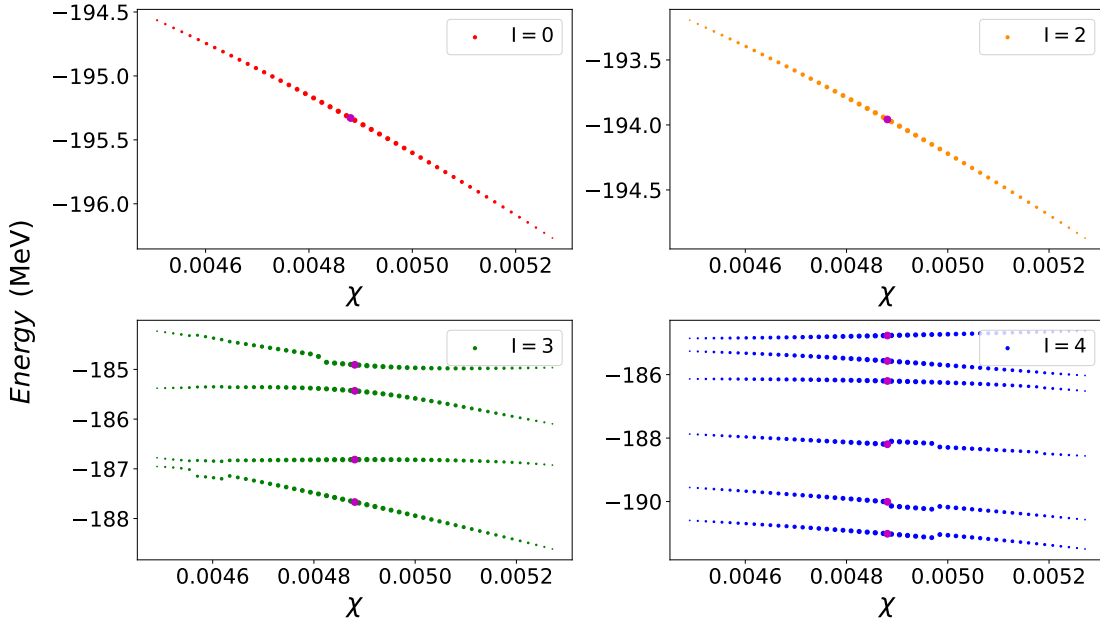


Figure 4: Change in energy levels of  $^{24}\text{Mg}$  with respect to a change in the quadrupole strength parameter  $\chi$ . The purple marker is the mean value of  $\chi$  resulting from the fitting procedure. Calculations performed with a small model of 4 harmonic oscillators and 10 HFB states.

The analysis assumes linearity around the parameter mean. We can see in Fig. 5 and Fig. 4,

that this can be reasonably achieved for even spins of  $N_{max} = 4$ , despite starting to accumulate non-linearities for  $\chi$  values further away from the mean.

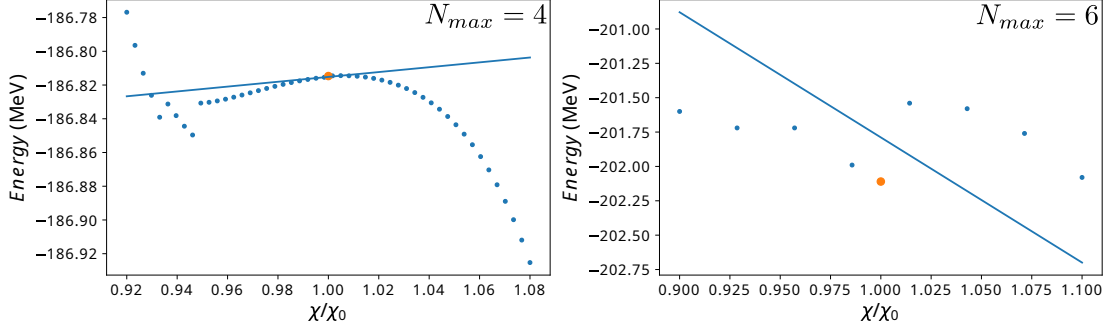


Figure 5: Variation in an energy state of  $^{24}\text{Mg}$  versus percentage change in  $\chi$ . The energy state  $I = 3$  on the left shows non-linear behavior as well as discontinuities at the edges of the  $\chi$  range. The  $I = 0$  state on the right shows a negative correlation. Linear best fit shown as a blue line. Mean value of parameter as an orange dot.

Whereas  $N_{max} = 6$  shows more non-linearly distributed points, despite a larger model. Although performing more calculations might reveal a more continuous distribution of points, what is more likely is that a calculation in a larger model space is slower to converge to an answer as the calculation is truncated at some point. Another explanation is that calculations with few basis states are unable to reproduce the physics of many-body interactions and what we see with the continuous points in  $N_{max} = 4$  is not physical. Despite this, we approximate the derivative by the fitted gradient with the justification that for a smaller model the variation in  $\chi$  was very linear. Moreover, this approach furthers the objective of developing the tools and concepts needed for further more computationally intensive analysis. Therefore we assume that there could be a linear relationship if the model was converged, and approximate this possible converged state by a linear fit. To calculate the derivatives we make a linear fit of the energy levels around the mean through all the points. This can be seen in Fig. 5.

Having calculated all the derivatives, we plot the variance in  $\chi$  calculated according to Eq. (7). We see that the error bars for the lowest state  $I = 2$  in  $N_{max} = 4$  and the second state for  $I = 3$  for  $N_{max} = 6$ , have a very small dependence on  $\chi$ , which can be seen by the error bars, that are much smaller when compared to all other states. This is likely only due to the widely distributed points for those states and does not indicate that the levels are truly independent of the choice of  $\chi$ .

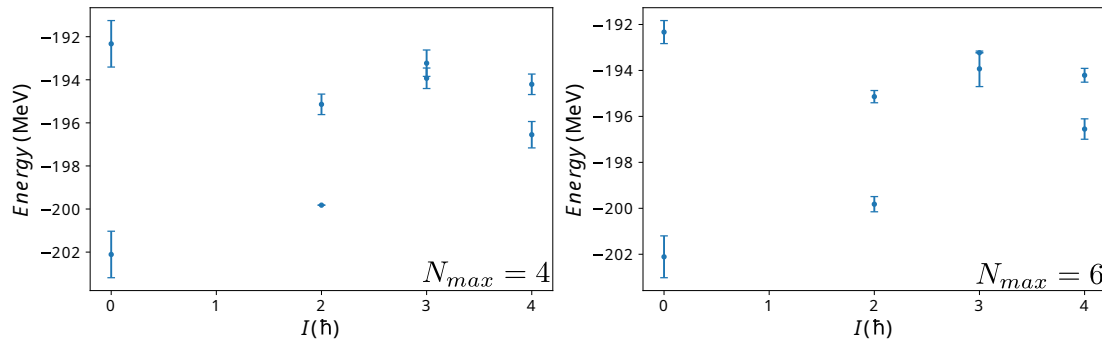


Figure 6: Energy levels of  $^{24}\text{Mg}$  with  $\sigma_{\tilde{\chi}}$  error bars for  $N_{max} = 4$  (left) and  $N_{max} = 6$  (right) with  $\Delta\tilde{\chi} = 0.1$ .

The error bars we have plotted in Fig. 6 do not represent true errors in the calculated spectrum, instead they represent the amount energy varies over a 10% range of  $\chi$  around 1, and show the general way the energy changes with a change in the parameter. A larger error bar shows that the value of  $\chi$  in that state needs to vary more to produce the same change in energy as a state smaller error bar. We see that the error for states  $I = 0$  is larger than the other states. This is reasonable as the deformation is determined by the shell nucleon being in a deformation driving orbital. In the plot we can see that the lowest state in  $I = 2$  is particularly less sensitive to variations in  $\chi$ .

### 3.1.2 Variation in $g$

The second parameter we vary is the pairing strength  $g$ . This parameter scales the pairing strength values  $g_p$  and  $g_n$ , determined in part 4 of the calculation. The range of  $g$  is 50% around the mean value. This is a larger range than that of  $\chi$ . There are 9 points of  $g$  values as the larger model needed to reproduce the pairing effects takes longer to run calculations.

We see in Fig. 7 that the variation in  $g$  is very non-linear. The pairing interaction seems to affect the energy mostly for values of  $g$  larger than 1. This possibly shows that for smaller values of  $g$  there is no formation of condensate, transition from the normal phase to a superfluid. Condensation is a critical process—meaning it only occurs if the pairing interaction is stronger than some threshold value [20]. Because of this we chose to fit the only the points which show condensate formation at values larger than 1.

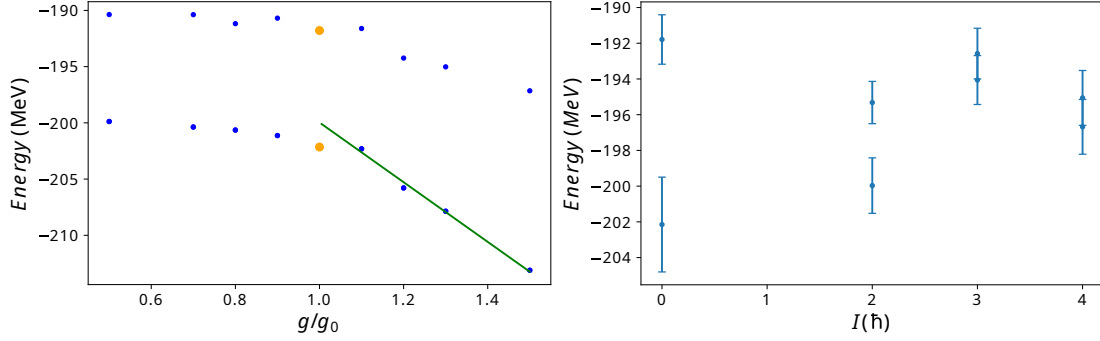


Figure 7: Two lowest  $I = 0$  states of  $^{24}\text{Mg}$  calculated with  $N_{max} = 6$  varying with  $g$  and the fitting procedure for variations in  $g$  on the left. Energy levels of  $^{24}\text{Mg}$  with  $\sigma_{\tilde{g}}$  error bars in  $g$  on the right, with  $\Delta\tilde{g} = 0.1$

In the right panel of Fig. 7 we have plotted the error bars calculated using Eq. (7). We observe again that the the lowest state for  $I = 0$  varies most with changes in  $g$  as the pairing interaction favors pairs of identical nucleons of angular momentum 0 as they have the largest overlap [21].

### 3.2 Covariance of $\chi$ and $g$

In this section we calculate the covariance values between  $\chi$  and  $g$ , then visualize them as error bars and covariance ellipses. The covariance matrices are calculated from the linear fit values in Section 3.1. Calculating the covariance matrix for a model with two variables by the approximation in Eq. (10) always produces a singular matrix. Take for example the case,

$$\mathcal{M} = \begin{bmatrix} \left(\frac{\partial E}{\partial g}\right)^2 & \frac{\partial E}{\partial \chi} \frac{\partial E}{\partial g} \\ \frac{\partial E}{\partial \chi} \frac{\partial E}{\partial g} & \left(\frac{\partial E}{\partial \chi}\right)^2 \end{bmatrix}. \quad (14)$$

Because the second derivatives are approximated by the first derivatives, the determinant of this matrix is 0 and it is not invertible. We chose instead to calculate the mixed derivatives as a finite difference

$$\frac{\partial^2 E}{\partial \chi \partial g} \approx \frac{\frac{\partial E}{\partial \chi} \Big|_{g=1.2} - \frac{\partial E}{\partial \chi} \Big|_{g=1}}{0.2}. \quad (15)$$

between the derivatives of energy with respect to  $\chi$  for a set of calculations at  $g = 1$  and  $g = 1.2$ . This gives us the covariance matrix estimate,

$$\hat{C} = \begin{bmatrix} \left(\frac{\partial E}{\partial g}\right)^2 & \frac{\partial^2 E}{\partial \chi \partial g} \\ \frac{\partial^2 E}{\partial \chi \partial g} & \left(\frac{\partial E}{\partial \chi}\right)^2 \end{bmatrix}^{-1} \approx \mathcal{M}^{-1}. \quad (16)$$

The analysis is done for the observables of energy  $E$  and the separation energy between the two lowest lying states  $T = E_1 - E_0$  for every value of  $I$ . The separation energy is the energy required

to excite one of the paired nuclei, breaking the pairing. In this way it is related to the pairing strength  $g$ .

Plotting the covariance ellipses as described in section 2.3.1, the covariance ellipse in Fig. 8 can be interpreted by considering changing the parameters along the respective axis. A shorter distance to the ellipse line implies a faster change in the given parameter. A highly skew ellipse e.g. angled at  $45^\circ$ , implies a strong covariance between the parameters, meaning that varying parameters together have a greater impact on the observable than individual parameter changes.

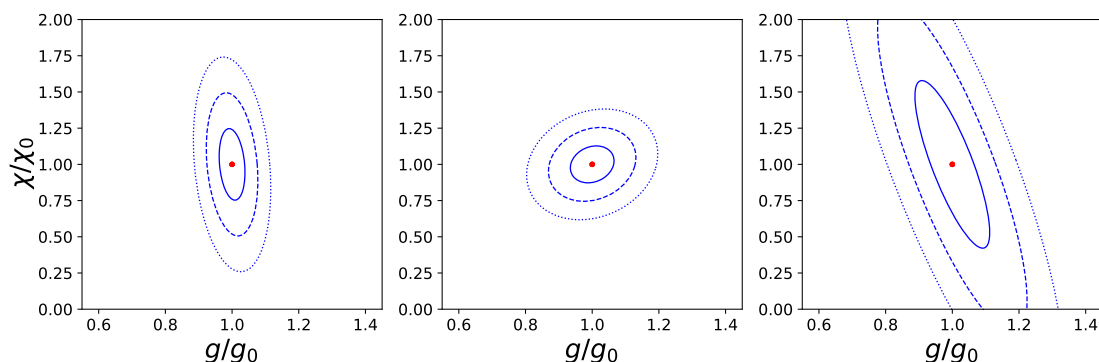
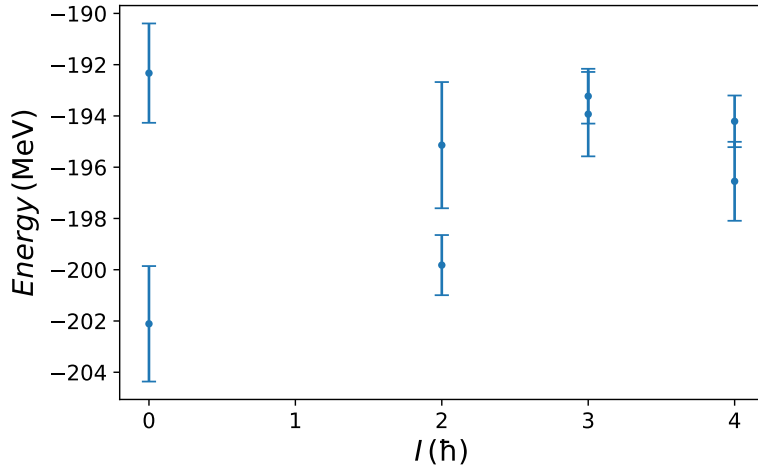


Figure 8: Covariance ellipses of  $E$  with respect to the parameters  $\chi$  and  $g$ . The ellipses bound a region of 1, 2 and 3  $\sigma$  change in energy as  $\chi$  and  $g$  are varied for  $I = 0, 2, 4$  respectively. Mean in red. The Pearson parameters are for  $I = 0$ :  $\rho = -0.22$ ,  $I = 2$ :  $\rho = 0.18$ ,  $I = 4$ :  $\rho = -0.81$ .

We see that the observable  $E$  has a very different behavior depending on the spin. For  $I = 0$  moving along the  $x$  axis, changing  $g$  affects  $E$  the strongest. As the covariance ellipse is mostly vertical, there is little covariance between the parameters—changing  $\chi$  and  $g$  simultaneously does not result in larger changes in  $E$  when compared to varying parameters individually.  $I = 2$  covariance ellipse shows that for this spin  $E$  is more sensitive to changes in  $\chi$  and there is some positive correlation between the parameters.  $I = 4$  has the lowest sensitivity to the parameters as the covariance ellipse is much larger. The dominant parameter is again  $g$  and there is slight negative covariance between  $g$  and  $\chi$ . The increased covariance of  $g$  and  $\chi$  again might be an effect of the increased deformation of the nucleus at larger values of  $I$ . For very large values of  $I$  the nucleus might experience pairing collapse, which would appear as reduction in the dependence on  $g$  [21].

We also plot the error bars calculated from the Hessian matrix according to Eq. (11) in Fig. 9. These are error bars of the units of energy considering variation of 10% of both  $\chi$  and  $g$ . The lowest energy state in  $I = 0$  has a larger variation with the parameters. This together with the information about contributions to errors in Fig. 12 which shows the significant contribution to the variance is from the pairing term shows again that 0 spin states pairing is dominant.



r

Figure 9: Total variance  $\sigma$  in energy levels  $E$  of  $^{24}\text{Mg}$  calculated with  $N_{max} = 6$ , with change in both  $g$  and  $\chi$  calculated using error propagation Eq. (11), with  $\Delta\tilde{\chi} = \Delta\tilde{g} = 0.1$ .

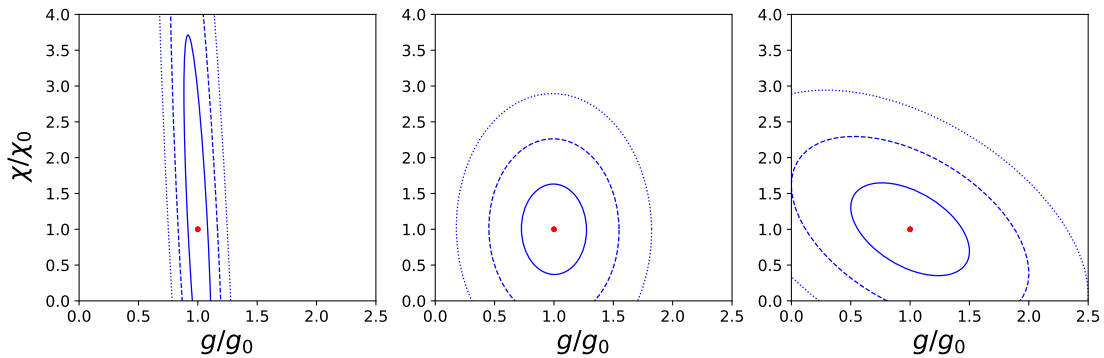


Figure 10: Covariance ellipses for  $T$  with respect to the parameters  $\chi$  and  $g$  of lowest lying states of  $^{24}\text{Mg}$  and  $I = 0, 2, 4$ . Concentric ellipses representing regions of 1, 2 and 3  $\sigma$  regions. Mean in red. The Pearson parameters are for  $I = 0$ :  $\rho = 13.2$ ,  $I = 2$ :  $\rho = 0.01$ ,  $I = 4$ :  $\rho = 1.96$ .

The Pearson coefficients we calculate for  $I = 0$  and  $I = 4$  have unreasonable values implying a larger than 100% correlation. This is due to the fact that for these spin values due to numerical errors the calculations presented non-linearities and there are very few points to calculate the gradient for. The gradient is nearly zero in  $\chi$ , while as the mixed derivative Eq. (15) gives a reasonable value. This shows that the analysis for  $T$  is not completely reliable yet. The covariance ellipses in Fig. 10 show that the change in separation energy  $T$  is greatest for the pairing strength parameter  $g$ , and there is little covariance of the parameters. This is expected as pairing directly affects the energy required to separate nucleons. For  $I = 2$  the variance in  $g$  is not as strong, but it is still the larger contribution.  $I = 4$  shows low variance in both  $\chi$  and  $g$  as well as a large degree of covariance between the parameters, as the ellipsis sits at an almost  $45^\circ$  angle, meaning the separation energy is more sensitive to variations in both parameters simultaneously. This

could be explained by the fact that for large  $I$  the nucleus is more deformed, which in turn leads to decreased effect of the pairing parameter.

Fig. 11 shows the variance in  $T$ , the difference between two lowest lying energy levels for the given spins calculated by Eq. (11).

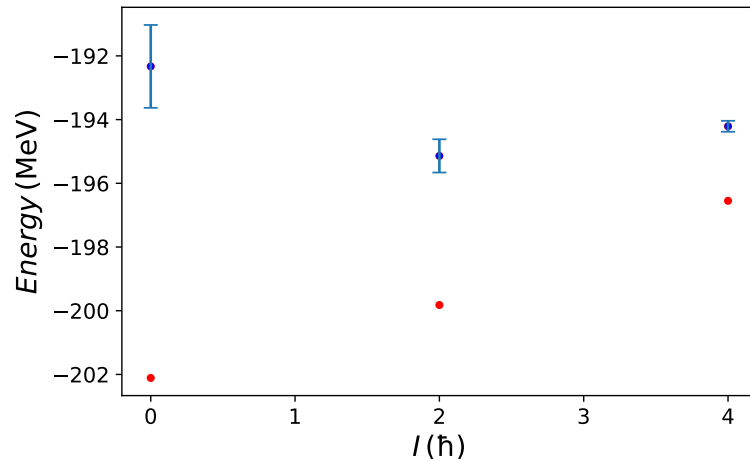


Figure 11: Total variance of excitation energy  $T$  for  $^{24}\text{Mg}$ . Red dots represent the ground state. The error bars  $\sigma$  are calculated using Eq. (11) with  $\Delta\tilde{\chi} = \Delta\tilde{g} = 0.1$ .  $0^+$  states in red.

We see that  $I = 0$  has a significantly stronger variance of  $T$ , which might again be explained by the sensitivity of less deformed states to changes in pairing strength.

Lastly we show the contributions to the total variance of energy and separation energy for the  $^{24}\text{Mg}$  calculations in Fig. 12 and Fig. 13. These are calculated by Eq. (11), the contribution from each parameter and the covariance of the two parameters being represented by a different color.

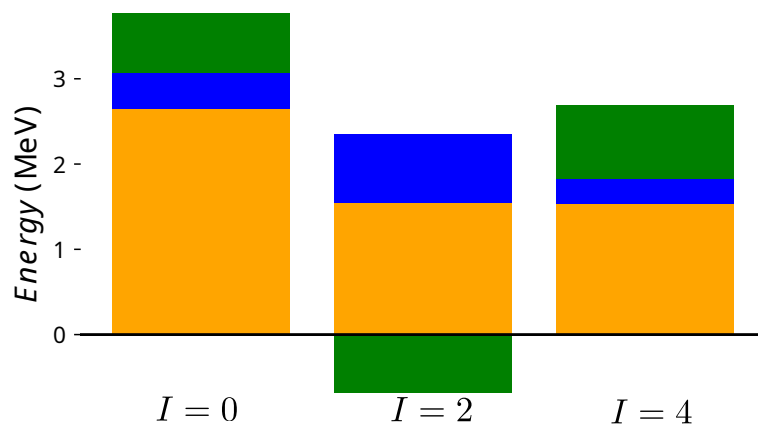


Figure 12: Graph of the contributions to the total variance of  $E$  for  $I = 0, 2, 4$  of  $^{24}\text{Mg}$ . Variation in  $\chi$ :  $\Delta\tilde{\chi} \partial^2 E / \partial \tilde{\chi}^2$  in blue,  $g$ :  $\Delta g \partial^2 E / \partial \tilde{g}^2$  in orange and the mixed contribution of varying  $\chi$  and  $g$  together:  $\Delta\tilde{\chi}\Delta\tilde{g} \partial^2 E / \partial \tilde{\chi}\partial \tilde{g}$  in green.

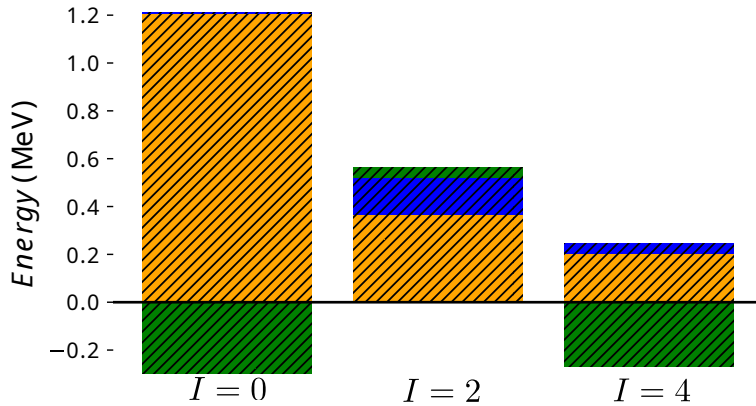


Figure 13: Graph of the contributions to the total variance of  $T$  in  $^{24}\text{Mg}$  for  $I = 0, 2, 4$ . Variation in  $\chi$ :  $\Delta\tilde{\chi} \partial^2 T / \partial \tilde{\chi}^2$  in blue,  $g$ :  $\Delta\tilde{g} \partial^2 T / \partial \tilde{g}^2$  in orange and the mixed contribution of varying  $\chi$  and  $g$  together:  $\Delta\tilde{\chi}\Delta\tilde{g} \partial^2 T / \partial \tilde{\chi}\partial \tilde{g}$  in green

We see that in general for separation energy  $T$  the dominant contribution is from the pairing parameter, contribution of which decreases rapidly for larger spins. The fact that the contribution from the covariance of  $\chi$  and  $g$  changes sign for every other even spin is likely coincidental.

Considering the analysis of both  $\chi$  and  $g$  shows that the changes in energy and separation energy are impacted greatly by the pairing term, but this strong dependence decreases when considering non-zero spins.

## 4 Conclusion and Outlook

In this thesis we have performed a basic error analysis for the Lund nuclear model. We focused on the case of  $^{24}\text{Mg}$  and performed calculations varying the effective Hamiltonian parameters  $\chi$  and  $g$ . Extrapolating the derivatives of the energy and separation energy observables, with respect to the parameters, to the variance in these observables we quantify the degree of dependence. Studying the covariance ellipses of the parameters we observe that for low spin states the parameters are largely uncorrelated. We expect this trend to be applicable for most low spin states of even-even nuclei. Nuclei with odd number of particles have different deformation characteristics, so this might not apply. The parameter  $\chi$  contributes less than  $g$  to the variance in both considered observables. The dominant contribution to the variance in the observables is in  $g$ , but it decreases in importance for states of higher spin. We relate this to the dependence of the pairing energy contribution to the overlap of 0 angular momentum nucleons. We also observe an increased effect of the covariance in  $\chi$  and  $g$  with larger spin. This can be due to a larger quadrupole deformation strength parameter leads to a larger deformation again breaking the time-reversal symmetry, resulting in a decreased effect of the pairing parameter.

As both the coupling constants are determined by fits to the reference functional one could

expand the analysis by incorporating the knowledge on statistical properties of these functionals, which have been calculated by e.g. Haverinen and Kortelainen [22]. Next, one could calculate the relationships between more observables of interest, such as the nuclear radii and shapes.

The analysis performed was very limited and depended on some assumptions forced by the limited computation resources. The analysis was performed under the assumption of linearity of the variation in parameters. We saw that this was not at all satisfied. The distribution of points for larger model spaces was quite chaotic. Given more time and computation resources one could increase the number of calculations and model size. This would give a greater accuracy of the estimates as well as a clearer picture of the true relation between the parameters. With more calculations one could also construct a statistical emulator, which outputs observables distributed so as to reproduce the performance of the nuclear model, without performing any computationally heavy calculations [23]. The findings presented in this thesis can be seen as a first step towards a method of calculating error estimates in the Lund model, taking as a starting point the methods described by Dobaczewski et al. [8]. This approach could be expanded and integrated into the code for the Lund model to estimate the errors for all calculations performed. This could be important when running calculations for larger nuclei, where the deviation from experiment can be even more significant.

The analysis could of course be expanded to other observables of interest for nuclei across the nuclear landscape. The radius, mass and predicted neutron skin sizes have been targets of previously performed analysis for other nuclear models. These might be good to calculate to compare to the performance of other models [8].

An alternative approach is the use of Bayesian statistics to combine observations of the model with knowledge of statistical distribution of the physical parameters of the system. In the Bayesian framework there are *priors* which encode our knowledge of the model affecting the *posterior* observable distributions. Bayesian statistics has a long history in physics going back to Laplace [19]. Some applications of Bayesian analysis have been model-mixing analysis to show how current theoretical models have difficulties reproducing mass measurements for  $^{80}\text{Zr}$  [24], and a method to combine many interaction parameterizations to arrive at more accurate estimates for properties of  $^{208}\text{Pb}$  [23]. The logical next step would be to first improve the techniques presented in this thesis, expanding the analysis to more variables. This would then be a good starting point to introduce some Bayesian techniques for faster and more accurate calculation of error estimates.

## References

- [1] I. Ragnarsson and S. Gösta Nilsson, “Shapes and shells in nuclear structure”, *Shapes and Shells in Nuclear Structure* (2005).
- [2] M. Zastrow, “In search for “magic” nuclei, theory catches up to experiments”, *Proceedings of the National Academy of Sciences* **114**, 5060–5062 (2017).
- [3] J. Stone and P.-G. Reinhard, “The skyrme interaction in finite nuclei and nuclear matter”, *Progress in Particle and Nuclear Physics* **58**, 587–657 (2007).
- [4] P. Ring and P. Schuck, *The nuclear many-body problem* (Springer Science & Business Media, 2004).
- [5] T. Skyrme, “The effective nuclear potential”, *Nuclear Physics* **9**, 615–634 (1958).
- [6] R. Furnstahl (for the UNEDF Council), “The UNEDF Project”, *Nuclear Physics News* **21**, 18–24 (2011).
- [7] E. Chabanat, P. Bonche, P. Haensel, J. Meyer, and R. Schaeffer, “New skyrme effective forces for supernovae and neutron rich nuclei”, *Physica Scripta* **1995**, 231 (1995).
- [8] J. Dobaczewski, W. Nazarewicz, and P.-G. Reinhard, “Error estimates of theoretical models: a guide”, *Journal of Physics G: Nuclear and Particle Physics* **41**, 074001 (2014).
- [9] J. Ljungberg, B. G. Carlsson, J. Rotureau, A. Idini, and I. Ragnarsson, “Nuclear spectra from low-energy interactions”, *Physical Review C* **106**, 10.1103/physrevc.106.014314 (2022).
- [10] T. Editors, “Editorial: uncertainty estimates”, *Phys. Rev. A* **83**, 040001 (2011).
- [11] A. Sâmark-Roth et al., “Spectroscopy along flerovium decay chains: discovery of  $^{280}\text{Ds}$  and an excited state in  $^{282}\text{Cn}$ ”, *Phys. Rev. Lett.* **126**, 032503 (2021).
- [12] J. J. Cowan et al., “Origin of the heaviest elements: the rapid neutron-capture process”, *Rev. Mod. Phys.* **93**, 015002 (2021).
- [13] J. Erler, C. J. Horowitz, W. Nazarewicz, M. Rafalski, and P.-G. Reinhard, “Energy density functional for nuclei and neutron stars”, *Phys. Rev. C* **87**, 044320 (2013).
- [14] R. Furnstahl, H.-W. Hammer, and A. Schwenk, “Nuclear structure at the crossroads”, *Few-Body Systems* **62**, 1–11 (2021).
- [15] S. Brandt, *Statistical and computational methods in data analysis*, 2., rev. ed. (North-Holland ; Amsterdam : 1976).
- [16] F. J. Fattoyev and J. Piekarewicz, “Accurate calibration of relativistic mean-field models: correlating observables and providing meaningful theoretical uncertainties”, *Phys. Rev. C* **84**, 064302 (2011).

- [17] K. Kumar and B. Sørensen, “Derivation of the radial dependence of the quadrupole force from a woods-saxon potential”, *Nuclear Physics A* **146**, 1–14 (1970).
- [18] L. Wasserman, *All of statistics: a concise course in statistical inference*, Springer Texts in Statistics (Springer New York, 2013).
- [19] D. Sivia and J. Skilling, *Data analysis: a bayesian tutorial* (OUP Oxford, 2006).
- [20] D. M. Brink and R. A. Broglia, *Nuclear superfluidity: pairing in finite systems*, Vol. 24 (Cambridge University Press, 2005).
- [21] J. Egido, P. Ring, S. Iwasaki, and H. Mang, “On the validity of the mean field approach for the description of pairing collapse in finite nuclei”, *Physics Letters B* **154**, 1–5 (1985).
- [22] T. Haverinen and M. Kortelainen, “Uncertainty propagation within the unedf models”, *Journal of Physics G: Nuclear and Particle Physics* **44**, 044008 (2017).
- [23] B. Hu et al., “Ab initio predictions link the neutron skin  $^{208}\text{Pb}$  to nuclear forces”, arXiv preprint arXiv:2112.01125 (2021).
- [24] A. Hamaker et al., “Precision mass measurement of lightweight self-conjugate nucleus  $^{80}\text{Zr}$ ”, *Nature Physics* **17**, 1408–1412 (2021).